

Section 6

Developments in global forecast models, case studies, predictability investigations, global ensemble, monthly and seasonal forecasting

Recent Improvements to the Met Office Global NWP Model *

Malcolm E. Brooks, Paul Earnshaw, Sean Milton and David Walters[†]
Global model development and diagnostics, NWP, Met Office, United Kingdom.

1 Introduction

In 2005, the Met Office made two major changes to the global Unified Model component of its operational NWP suite. In January, a package of improvements was made to the model physics[1], and in December, the resolution was enhanced in both the horizontal and the vertical directions[2].

2 HadGEM 1 Physics Package

The January physics package included revisions to the boundary layer parametrisation and large-scale precipitation scheme microphysics, a change to increase the Saharan albedo and some corrections and revisions to the convection scheme. Most of these changes were part of a physics package tested and successfully implemented in the latest climate version of the Unified Model, HadGEM1.

The boundary layer (BL) changes were mainly improvements to the diagnosis of mixed layer depths in the decoupled stratocumulus regime and the main change to the convection scheme was a reduction of the CAPE closure adjustment timescale from 1 hour to 30 minutes (not currently in HadGEM1). The main impacts from these two changes are in the tropics. There is reduced oceanic tropical precipitation and an increase in precipitation over tropical land masses, both of which correct known systematic errors in tropical precipitation. These changes in precipitation are accompanied by improvements in the tropical large-scale circulation. The new BL scheme (the 8B scheme) also reduces low cloud over subtropical oceans, which improves the radiation balance in comparisons with ERBE and GERB (Meteosat 8).

The changes to the microphysics scheme (the 3C scheme) were numerous. Increased autoconversion of liquid water to precipitation helps dissipate excessive low cloud in the model, with improvements in near

surface temperatures. Also, an increased tendency to form ice means that it falls out more quickly, leading to a beneficial reduction in cloud over the poles. Finally, comparisons with ERBE and GERB top of atmosphere clear sky radiation budgets suggested that the Saharan surface albedo was previously underestimated, leading to excessive sensible heating of the surface. A change was made to increase Saharan albedo via the soil parameters, which gives an improvement to the radiation budget and reduces circulation errors over the region. The impact on RMS errors in parameters that make up the Met Office's "NWP index" skill-score are shown in Table 1.

3 40 km/50 Level Resolution

The resolution enhancement of the global NWP model was part of a wider project to increase model resolutions throughout the Met Office's NWP suite in 2005/6. The number of grid-points in the horizontal lat-lon grid was increased by about 48%, to 640(EW)×481(NS); this gives a physical resolution of approximately 40km at mid-latitudes. A plot of the result-

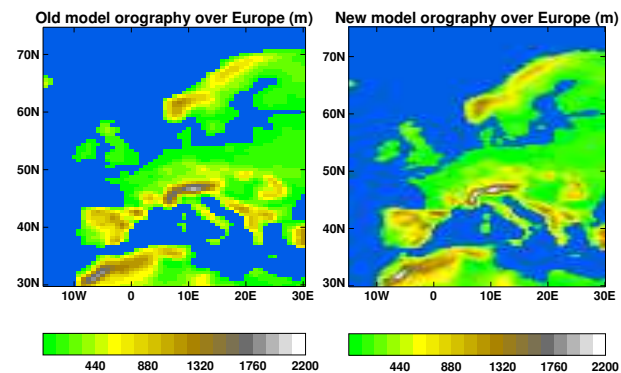


Figure 1: A comparison of the European orography in the old (left) and upgraded (right) global models, showing the improved resolution of coastlines and mountain ranges resulting from the finer horizontal grid.

ing orography over Europe, showing improved barrier

* ©British Crown Copyright, 2006.

[†]Corresponding author: david.walters@metoffice.gov.uk

heights for the Alps and Pyrenees, is illustrated in Fig. 1. In the vertical, the number of model levels has been increased from 38 to 50. The main focus was a better representation of the upper atmosphere, with a finer level structure in the stratosphere and an increase in the height of the model lid from 39 km to 63 km, i.e. from the upper stratosphere to the lower mesosphere. This not only allows for the better assimilation of satellite data, but improves the Met Office’s capability in stratospheric forecasting, by superseding the climate-resolution 50 level forecast model dedicated to this purpose. A comparison between the old and new level sets is made in Fig. 2. A further

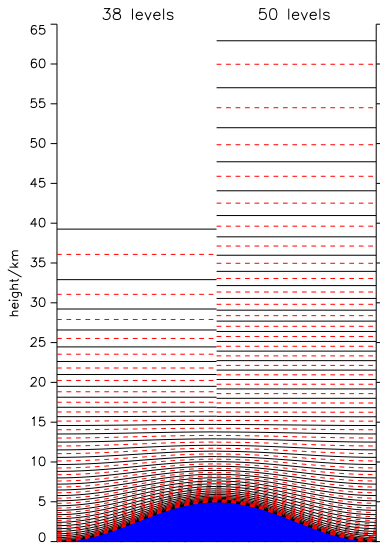


Figure 2: A comparison of the level sets in the old (left) and upgraded (right) global models. The majority of extra levels can be seen to be in the stratosphere.

increase to 70 levels in 2007 will focus on improvements to the representation of the boundary layer and the troposphere. Finally, to compliment these increases in spatial resolution, the model timestep was decreased from 20 to 15 minutes.

The main improvements in model performance come from the increased number of levels and the increase in the height of the model lid, with a decrease in both RMS errors and biases in geopotential heights, temperatures and winds at mid-to-upper levels. We also see a decrease of random error in lower-level fields such as PMSL in 1-3 day forecasts. Whilst the impact of the finer horizontal grid on the RMS-based NWP skill-scores is fairly modest, it does lead to some improvement in the tropics, including better wind forecasts, a weaker Hadley circulation and

reduced precipitation over the oceans. More importantly, the increased resolution also allows for a better representation of small-scale features. This leads to a beneficial increase in eddy kinetic energy and to the development of systematically deeper tropical cyclones compared to the old 60km model. The impact on errors in components of the NWP index are shown in Table 1.

Field	RMSE Difference Test-Cont (%)	
	HadGEM Ph. ¹	40km 50L
T+24 NH PMSL	-1.0	0.12
T+48 NH PMSL	-1.1	-2.04
T+72 NH PMSL	-1.9	-1.31
T+96 NH PMSL	-0.7	0.23
T+120 NH PMSL	-0.9	2.80
T+24 NH 500 HGT	-1.0	-1.75
T+48 NH 500 HGT	-1.3	-2.69
T+72 NH 500 HGT	-0.7	-2.08
T+24 NH 250 Wind	-0.7	-0.59
T+24 Tr. 850 Wind	-2.3	-0.63
T+48 Tr. 850 Wind	-3.7	-0.41
T+72 Tr. 850 Wind	-4.7	-0.81
T+24 Tr. 250 Wind	-0.4	0.33
T+24 SH PMSL	-2.7	1.89
T+48 SH PMSL	-4.1	1.56
T+72 SH PMSL	-4.7	0.25
T+96 SH PMSL	-4.1	-2.02
T+120 SH PMSL	-3.4	-5.19
T+24 SH 500 HGT	-0.4	-1.13
T+48 SH 500 HGT	-1.3	-1.80
T+72 SH 500 HGT	-2.4	-6.08
T+24 SH 250 Wind	-1.0	1.31
Δ NWP index (points)	2.25	0.99

Table 1: Impact on RMSE for parameters that make up the NWP Index. Verification of the physics and resolution changes against observations are from 1 month trials in Winter 2003/4 and Winter 2004/5 respectively.

References

- [1] Milton, S. *et al.* HadGEM1 physics for the global NWP model (cycle G34): Improvements to boundary layer, large scale precipitation, convection and saharan albedo. Technical Report 458, NWP, Met Office, UK (2005).
- [2] Earnshaw, P., Milton, S. & Walters, D. Enhanced vertical and horizontal resolution in the global NWP model (cycle Gxx). Technical Report In Preparation, NWP, Met Office, UK (2006).

¹Data only available to $\frac{1}{7}$ % accuracy.

Improvements in the Prediction of the Diurnal Cycle of Clouds Using Multimodels and a Unified Cloud Scheme

Arindam Chakraborty* T. N. Krishnamurti C. Gnanaseelan
Dept. of Meteorology, Florida State University, Tallahassee, FL 32306

Clouds are important components of radiation budget of the atmosphere. Precipitation and cloudiness show highest amplitude of variation at time period of one day. In this study it has been shown that the forecasting of the diurnal cycle of clouds can be greatly improved using a multimodel superensemble (SE) (Krishnamurti et al. 1999). Further, a unified cloud parameterization scheme (Unf) is developed based on the idea of SE. All the results are validated against the International Satellite Cloud Climatology Project (ISCCP) infrared data sets (Schiffer and Rossow 1983).

Four versions of the Florida State University (FSU) atmospheric global spectral model (GSM) were used with four different cloud parameterization schemes at T126L28 resolution ($\sim 0.94^\circ$ and 28 vertical sigma layers). 5-day long forecasts were made from 1 January 2000 to 31 March 2000. Superensemble forecasts from these models were created for the last 10 days using training statistics of the first 81 days. The Unf used the statistics of the 4 versions of the models from 1 January 2000 to 28 February 2000. The model forecasts with this new scheme were made for 1 to 31 March 2000.

The total diurnal cycle of low, middle and high clouds over the entire tropical ($0-360^\circ\text{E}$, $30^\circ\text{S}-30^\circ\text{N}$) land and ocean is shown in Fig 1 for day-4 of forecasts. Low clouds over the tropics show a peak at 12 hours local time over land and at 09 hours local time over ocean. Most of the member models have great difficulty in predicting the phase and amplitude of low clouds both over land and ocean. The Unf and the SE greatly improved the error of the diurnal cycle of low clouds over land and ocean.

Middle clouds show a peak at 03 hours over land and at 00 hours over ocean. Only one member model is able to show this phase and amplitude of middle clouds somewhat correctly (Fig 1c, d). The RMS error of the total diurnal cycle was reduced by 3 to 5 times with the use of the Unf and the SE.

High clouds show peak at 21 hours over land and at 15 hours over ocean (Fig 1e, f). All the models and their ensemble mean (EM) were unable to forecast the phase and amplitude of high clouds. The phase error of the models were large over ocean as compared to over land. The skills of the Unf and the SE were much higher compared to all the member models and their EM.

Phase and relative amplitude of high clouds from ISCCP, EM, Unf and SE over the Amazon region is shown in Fig 2 for day-4 of forecasts in vector representation. It can be noticed that both the phase and amplitude of the diurnal cycle were improved using the Unf and the SE. The domain average absolute phase error for the EM is 2.9 hours, and that for the Unf and SE are 1.8 and 2.0 hours respectively.

These results show that SE can improve the diurnal cycle of cloud covers to a great extent. The newly developed unified cloud scheme also shows much higher skill in predicting the phase and amplitude of diurnal cycle of clouds. This scheme should be tested in real time numerical weather prediction models.

*arch@io.met.fsu.edu

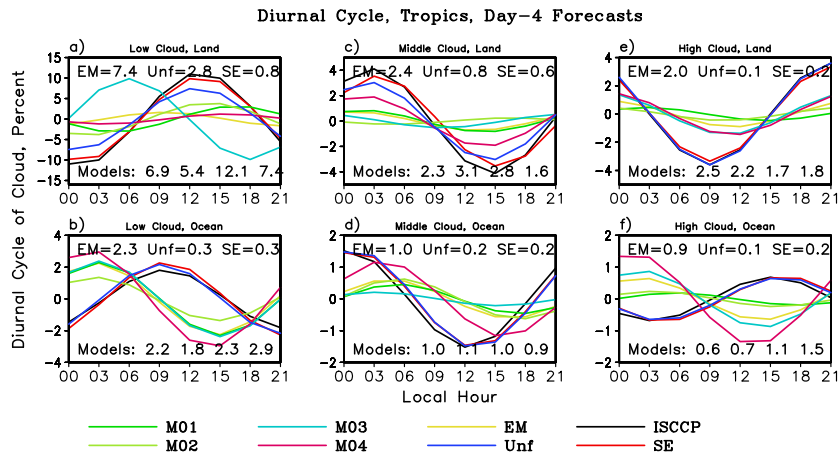


Figure 1: Diurnal cycle of low, middle and high cloud cover over the Tropics (0° – 360° E, 30° S– 30° N) from ISCCP and day-4 forecasts from the member models, ensemble mean (EM), unified scheme (Unified) and the superensemble (SE) during 22–31 March 2000. RMS error (in percent) of the total diurnal cycle for EM, Unified and SE are indicated at the top of the panels, and those for the member models are shown at the bottom of the panels.

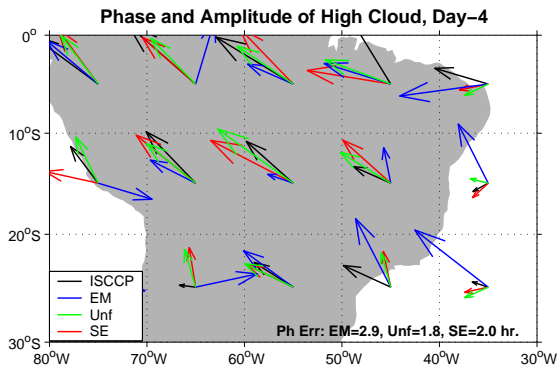


Figure 2: Phase and amplitude of the diurnal cycle of high cloud cover over the Amazon region from ISCCP and day-4 forecasts from the ensemble mean (EM), unified scheme (Unf) and the superensemble (SE) during 22–31 March 2000. A northward arrow represents a phase at 00 hours and eastward arrow represents a phase at 09 hours.

References

- Krishnamurti, T. N., C. M. Kishtawal, T. E. LaRow, D. R. Bachiochi, Z. Zhang, C. E. Williford, S. Gadgil, and S. Surendran, 1999: Improved weather and seasonal climate forecasts from multimodel superensemble. *Science*, **285**, 1548–1550.
- Schiffer, R. A., and W. B. Rossow, 1983: The International Satellite Cloud Climatology Project (ISCCP): The first project of the World Climate Research Programme. *Bull. Amer. Meteor. Soc.*, **64**, 779–784.

Seasonal forecast skill increase due to vertical resolution

Michel Déqué and Jean Philippe Piedelievre
Météo-France/CNRM Toulouse, France. deque@meteo.fr

Evaluation of the skill of seasonal forecasts is a computationally expensive exercise, as the number of years must be at least 10 for tropics and 30 for midlatitudes. The size of the ensembles must be at least 3 for the tropics and 9 for midlatitudes. Otherwise, the accuracy of the scores is too poor (Déqué, 1997). The choice of horizontal and vertical resolution is a compromise between the expected improvement and the cost of a reliable evaluation experiment. In the PROVOST European project (Doblas-Reyes et al., 2000), an attempt to introduce high resolution in the stratosphere was not successful in terms of score improvement. Possible reasons were the number of stratospheric levels (20), the absence of coupling with the ocean, the poor quality of the ERA15 analyses in the stratosphere.

In the DEMETER European project (Palmer et al., 2004), the conditions are more favorable: the 44 years of ERA40 offer a good dataset for stratospheric initial conditions, and the forecast exercise is carried out in coupled mode. The experiment we present here is based on a revisit of the winter forecasts with a more recent version of one of the participating models. We used version 4.4 of ARPEGE-Climate (Déqué, 2003). The initial atmospheric conditions are obtained from ERA40 data, whereas the ocean is initialized by an uncoupled run of the model forced by the daily ERA40 surface fluxes. Nine members, obtained by lagging by using the last 9 days of October as an atmospheric initial condition, have been produced for 44 winters (starting at 1st November 1958 through 2001). The standard simulation uses 31 vertical levels, as in DEMETER. Although the model has undergone a few improvements since the original DEMETER exercise (the forecast scores are improved in uncoupled mode), this new version is generally below the original one in terms of scores.

A stratospheric version has been built by using 91 levels and letting ozone evolve as a prognostic variable (it is prescribed from a multi-year average of the same field in the 31L version). In addition the time step is divided by two to maintain time stability. As a result of the quadratic increase of the radiative calculations, the 91L version is ten times more expensive than its 31L counterpart. Table 1 indicates the average pressure in the middle of each layer for both resolutions. The anomaly correlation of both models has been calculated for the DJF (month 2-4) averages with respect to the ERA40 values. Except in the southern hemisphere, the scores are significantly improved. This result is in agreement with recent findings of Baldwin et al. (2003) about stratospheric memory.

References:

Baldwin, M.P., Stephenson, D.B., Thompson, D.W.J., Dunkerton, T.J., Charlton, A.J. and O'Neill, A., 2003: Stratospheric memory and extended-range weather forecasts. *Science*, 301, 636-640.

Déqué, M., 1997: Ensemble size for numerical seasonal forecasts. *Tellus*, 49A, 74-86.

Déqué, M., 2003: Documentation of ARPEGE-Climate version 4. Available electronically in 3 volumes upon request to the author.

Doblas-Reyes, F.J., Déqué, M. and Pledelievre, J.P., 2000: Model and multimodel spread in the PROVOST seasonal forecasts : application to probabilistic forecasts. *Quart. J. Roy. Meteor. Soc.*, 126, 2069-2088.

Palmer, T.N., Alessandri, A., Andersen, U., Cantelaube, P., Davey, M., Délecluse, P., Déqué, M., Díez, E., Doblas-Reyes, F.J., Feddersen, H., Graham, R., Gualdi, S., Guérémy, J.F., Hagedorn, R., Hoshen, M., Keenlyside, N., Latif, M., Lazar, A., Maisonnave, E., Marletto, V., Morse, A.P., Orfila, B., Rogel, P., Terres, J.M. and Thomson, M.C., 2004: Development of a European Multi-Model Ensemble System for Seasonal to Inter-Annual Prediction (DEMETER). Bull. Am. Meteorol. Soc., 85, 853--872.

0.01	0.03	0.06	0.10	0.17	0.28	0.43	0.64	0.92	1.30
1.78	2.38	3.12	4.02	5.09	6.34	7.80	9.47	11.37	13.50
15.88	18.52	21.41	24.57	27.99	31.67	35.63	39.85	44.33	49.07
54.07	59.31	64.80	70.51	76.43	82.57	88.96	95.61	102.58	109.88
117.58	125.72	134.35	143.52	153.25	163.58	174.52	186.13	198.42	211.44
225.23	239.82	255.26	271.58	288.85	307.09	326.37	346.74	368.24	390.94
414.88	440.11	466.51	493.86	521.90	550.35	578.95	607.46	635.74	663.68
691.15	718.01	744.13	769.39	793.68	816.90	838.92	859.65	879.04	897.00
913.47	928.41	941.82	953.68	964.00	972.80	980.35	986.78	991.98	995.95
998.82									
10.00	30.00	50.00	70.00	90.08	110.64	132.32	155.60	180.77	208.01
237.35	268.76	302.17	337.46	374.50	413.17	453.32	494.84	537.57	581.36
626.02	671.31	716.89	762.33	807.04	850.23	890.88	927.68	958.96	982.63
996.14									

Table 1: Vertical discretization (hPa) of the 91L version (row 1-10) and of the 31L version (row 11-14)

		Globe	NH	SH	Tropics	Nino3.4
Z500	31L	.20	.12	.17	.64	.25
	91L	.25	.20	.16	.67	.41
Precip.	31L	.45	.14	.07	.47	.58
	91L	.51	.19	.04	.53	.72
S Temp.	31L	.25	.16	.22	.40	.47
	91L	.30	.23	.23	.42	.51

Table 2: Anomaly correlations of 500 hPa height, precipitation and surface temperature in the two vertical resolutions. The verification domains are the globe, the northern hemisphere (30°N-90°N), the southern hemisphere (30°S-90°S), the tropics (30°S-30°N) and the Nino3.4 box (5°N-5°S, 120°E-170°E).

Global NWP Superensemble from multimodels

T. N. Krishnamurti and Akhilesh K. Mishra

Department of Meteorology Florida State University Tallahassee, FL-32306

Email: tnk@io.met.fsu.edu, akhil@io.met.fsu.edu

Florida State University maintains a real time global NWP superensemble from multimodels following the works of Krishnamurti et al. (2000, 2001, 2003). The multimodels include day 1 through day 6 of forecast from 7 forecast models namely ECMWF model (European Centre for Medium-Range Weather Forecasts 2.5 deg res.) GFS model (National Centers for Environmental Prediction USA, NCEP) JMA Global Spectral Model (Japan Meteorological Agency, JMA) GEM model (Canadian Meteorological Centre, CMC/RPN) NOGAPS (Fleet Numerical Meteorology and Oceanography Center, FNMOC/NRL) GASP model (Australian Bureau of Meteorology, BMRC) and FSU Global Spectral Model (Florida State University, FSU). This superensemble is constructed from multimodel data at a horizontal grid resolution of T126 (120 waves triangular truncations) which carried a transform grid separation of roughly 90 Km). This procedure entails a training phase (covering the past forecast of same 120 recent days) and a real time forecast phase. One forecast per day at 12 UTC is issued by Florida State University. The training phase extracts the error statistics of the member models and those are used to arrive at a consensus forecast called the Superensemble. In the enclosed illustrations (Fig. 1) the recent diagnostic and probabilistic skill scores, RMS errors, anomaly correlations and equitable threat scores and bias (for precipitation) are evaluated on a regular basis to examine the NWP forecast skills regionally and globally for the member model of the suite, ensemble mean and of the multimodel superensemble. The salient aspects of this forecast are that the FSU superensemble invariably provides the best global and regional forecasts up to 6 days. The threat scores for light (2mm/day) as well as heavy rains (5mm/day) are best provided by this system. The same is seen for the RMS errors and anomaly correlations for all variables (500 hPa geopotential heights and MSLP are shown in Figure 1). Enclosed diagram illustrates the anomaly correlation and the RMS errors for the sea level pressure (a) and (b), 500 hPa level geopotential heights (c) and (d), equitable threat score and BIAS calculated for the 2mm/day and 5 mm/day threshold (e through h) for the month of June (2005) over the globe.

Basically forecasts for all these elements show very high skills for the multimodel superensemble that is shown by the dark bars. These carry the highest anomaly correlation and the lowest RMS errors for each of the forecast days. Here the skills for 7 of the best models are compared with the superensemble (far right) and ensemble means (shown next to the superensemble). The results of the superensemble appear clearly better than those of the ensemble mean. The most striking results are the large improvements in the anomaly correlation from the multimodel superensemble, values as high as 0.90 to 0.94 on day 4 of the forecast are worth noting.

References

1. Krishnamurti, T.N., C.M. Kishtawal, T. LaRow, D. Bachiochi, Z. Zhang, C.E. Williford, S. Gadgil and S. Surendran, 2000: Multimodel superensemble forecasts for weather and seasonal climate. *J. Climate*, **13**, 4196-4216.
2. Krishnamurti, T.N., S. Surendran, D.W. Shin, R.J. Correa-Torres, T.S.V. Vijaya Kumar, C.E. Williford, C. Kummerow, R.F. Adler, J. Simpson, R. Kakar, W.S. Olson, and F.J. Turk, 2001: Real-time multianalysis-multimodel superensemble forecasts of precipitation using TRMM and SSM/I products. *Mon. Wea. Rev.*, **129**, 2861-2883.
3. Krishnamurti, T.N., K. Rajendran, T.S.V. Vijaya Kumar, S. Lord, Z. Toth, X. Zou, S. Cocke, J.E. Ahlquist, I.M. Navon, 2003: Improved skill for the anomaly correlation of geopotential heights at 500 hPa. *Mon. Wea. Rev.*, **131**, 1082-1102

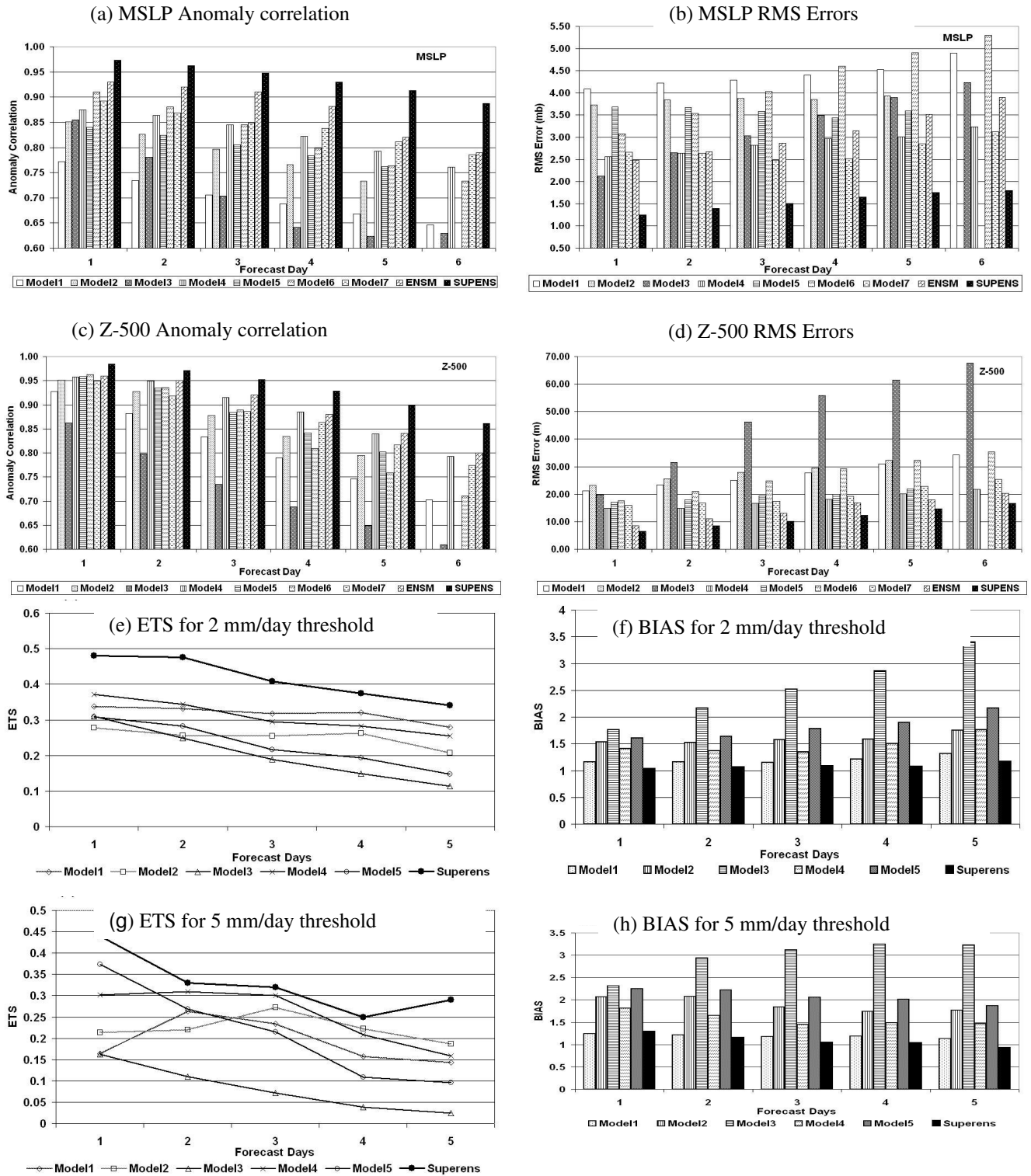


Figure 1. Skill scores of Operational FSU Multimodel Superensemble for June 2005 (a) MSLP Anomaly correlation, (b) MSLP RMS Errors, (c) z-500 Anomaly Correlation, (d) z-500 RMS Errors, (e) Equitable threat score (ETS) for 2mm/day threshold, (f) BIAS for 2mm/day threshold, (g) ETS for 5mm/day threshold and (h) BIAS for 5mm/day threshold.

Introduction of the Reduced Gaussian Grid into the Operational Global NWP Model at JMA

Kengo Miyamoto*†

*Advanced Earth Science and Technology Organization

†Numerical Prediction Division, Department of Forecast, Japan Meteorological Agency

1. Introduction

JMA (Japan Meteorological Agency) plans to upgrade the spatial resolution of the operational global spectral NWP model from T_{L319} to T_{L959} . In order to realize this, we are going to introduce the reduced Gaussian grid into the model. On the standard Gaussian grid, when the latitude is higher, the longitudinal interval between two grid points is smaller. However, especially in the polar region, all of grid points are not so necessary. Therefore, we wish to reduce the redundant grid points, in order to save the computational throughput. This article describes the determination of the necessary number of longitudinal grid points at each latitude and the sustained accuracy of the model with the reduced Gaussian grid system.

2. Reduction Strategy of the Number of Grid Points

In order to determine the necessary number of longitudinal grid points at each latitude, we adopt the reduced spectral transformation introduced in Juang (2004). Since our global atmospheric model is a spectral model, some calculations are processed in grid space and the others are processed in wavenumber space. The variables in the model experience a wave-to-grid transformation and a grid-to-wave transformation in each time step. In the standard spectral transformation which is used in the model with the standard Gaussian grid system, the Legendre transformations use all of wavenumber components corresponding to the higher left half of the upper three squares in Figure 1. However the values in the purple region are negligibly small compared with those in the red region. The lower three squares in Figure 1 concern the reduced spectral transformation which is used in the model we are now developing. In the reduced spectral transformation, the Legendre transformations only use the wavenumber components for which the associated Legendre function has significant value (grater than the machine epsilon). Obviously, we can define the maximum longitudinal wavenumber for each latitude. Resting on this maximum longitudinal wavenumber, we evaluate the necessary number of longitudinal grid points for each latitude. The total number of grid points can be curtailed by about 30% in the case of T_{LR959} (Figure 2).

3. Performance in the Shallow Water Experiment

A simplified experiment is performed to examine the accuracy of the reduced spectral transformation. The shallow water equation in advective form is integrated for 14 days on the core of the T_{R639} reduced quadratic Gaussian grid (T_{R639}) with an Eulerian advection scheme. The initial condition is a zonal flow with the corresponding surface height field (one of steady state solutions to the non-linear shallow water equation; same as in the second test case by Williamson et al., 1992). In Figure 3, we are not able to distinguish the initial state and the state after 14-day integration, concerning with the surface height and the zonal velocity. Regarding the meridional velocity, the difference is discernible. Since the true meridional velocity is always zero, the red plot shows the distribution of the error. However, because the scale of the ordinate is 10^{-11} times smaller than that of the zonal velocity, we are able to recognize that the steady state could be kept during 14-day integration and the reduced spectral transformation which we adopt has enough accuracy for practical daily weather forecasts.

†Corresponding author address: Dr. Kengo Miyamoto, Numerical Prediction Division, Department of Forecast, Japan Meteorological Agency, 1-3-4 Otemachi, Chiyoda-ku, Tokyo 100-8122, Japan.
E-mail: miyamoto@naps.kishou.go.jp

References

- Juang, H.-M.H., 2004: A Reduced Spectral Transform for the NCEP Seasonal Forecast Global Spectral Atmospheric Model. *Mon. Wea. Rev.*, **132**, 1019-1035.
- Williamson, D.L., J.B. Drake, J.J. Hack, R. Jakob and P.N. Swarztrauber, 1992: A Standard Test Set for Numerical Approximations to the Shallow Water Equations in Spherical Geometry. *J. Comput. Phys.*, **102**, 211-224.

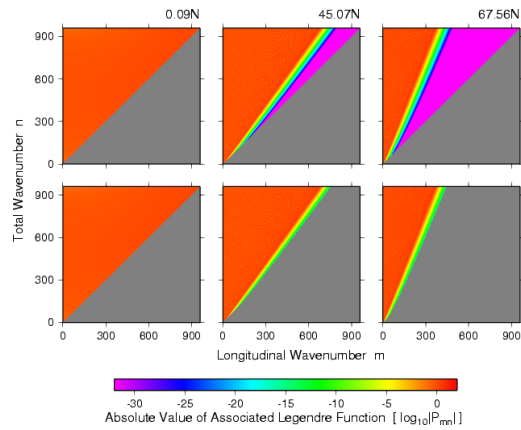


Figure 1: The absolute values of the associated Legendre function on three latitudes, near the Equator, in the middle latitudes, and in the high latitudes. The upper (lower) three squares concern the standard (reduced) spectral transformation. The abscissa (ordinate) is the longitudinal (total) wavenumber. There are not any values in the gray hatched lower right half of each square.

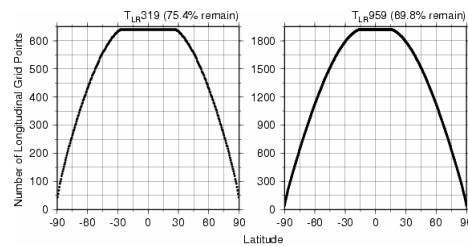


Figure 2: The necessary number of longitudinal grid points for each latitude. JMA plans to use T_{LR319} (left panel) for the inner model of the 4D-Var data assimilation system and T_{LR959} (right panel) for the forecast model.

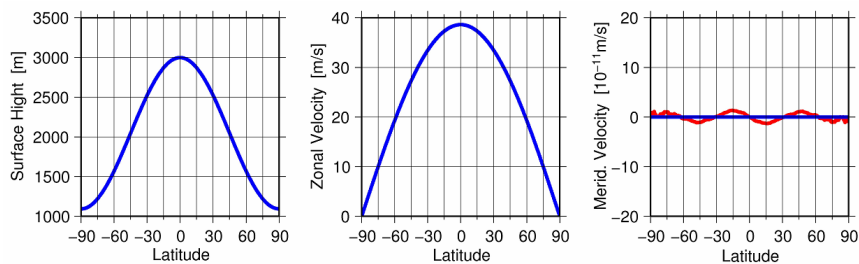


Figure 3: The Latitudinal distributions of the surface height (left), the zonal velocity (middle), and the meridional velocity (right) at Greenwich meridian in a simplified experiment performed with a shallow water model of T_{R639} . The blue plots show the initial values on each field. The red plots show the values after 14-day integration.

Long-Term Winter Rainfall Predictions Over the Southeast U.S. Using the FSU Global Spectral Model

Dawn C. Petraitis*, T. E. LaRow, and J. J. O'Brien

Center for Ocean-Atmospheric Prediction Studies, Florida State University, Tallahassee, FL

1. Introduction

The prediction of El Niño-Southern Oscillation (ENSO) teleconnection patterns by global models is important for regional climate simulations. In an effort to improve ENSO predictions using improved model physics, the skill of the Florida State University Global Spectral Model (FSUGSM) is assessed focusing on seasonal rainfall over the Southeast U.S. since precipitation patterns over the region have been found to be connected to ENSO (Ropelewski and Halpert, 1986).

2. Data and Methodology

The FSUGSM is a global spectral model with a T63 horizontal resolution (approximately 1.875°) and 17 unevenly spaced vertical levels. Details of this model can be found in Cocke and LaRow (2000). The experiment utilizes two runs using the Naval Research Laboratory (NRL) RAS convection scheme and two runs using the National Centers for Environmental Prediction (NCEP) SAS convection scheme to comprise the ensemble. The two convection schemes are slightly different in how they calculate cumulus cloud cover and convert that into precipitation. The simulation was done for 49 years, from 1950 to 1999. Reynolds and Smith monthly mean sea surface temperatures (SSTs) from 1950-1999 provide the lower boundary condition. Atmospheric and land conditions from 1 January 1987 and 1 January 1995 were used as the initial starting conditions. The observational precipitation data being used as the basis for comparison is a gridded global dataset from Willmott and Matsuura (2005). Monthly precipitation data for the boreal winter season (DJF) were averaged to create seasonal averages. A model ensemble was created using an equal-weight average of the four model runs. Temporal correlations between the observations and model data and between the average SST over the tropical Pacific and Southeast precipitation were calculated.

3. Results

Model ensemble correlations yield an insight into the overall skill of the models. Figure 1 shows the ensemble correlations to the observations for the ENSO signal, El Niño, and La Niña. The ENSO signal correlation (Figure 1a) is a combination of the warm and cold years as classified by the JMA ENSO index (JMA 1991). This particular correlation gives a general idea of how well the models represent the overall ENSO signal. The ENSO signal is then broken down into El Niño (Figure 1b) and La Niña (Figure 1c). The ensemble correlates well in the sensitive coastal areas, especially in the overall ENSO signal and El Niño. Since La Niña lacks a coherent pattern,

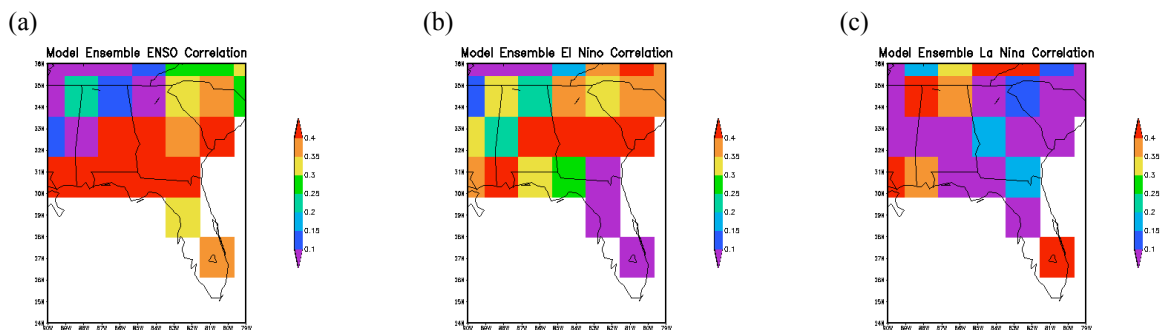


Figure 1: Temporal correlations showing areal patterns of the model ensemble for a) the overall ENSO signal, b) El Niño, and c) La Niña.

Corresponding author address: Dawn C. Petraitis, Center for Ocean-Atmospheric Prediction Studies, Florida State University, Tallahassee, FL 32306-2840
E-mail: dawn@coaps.fsu.edu

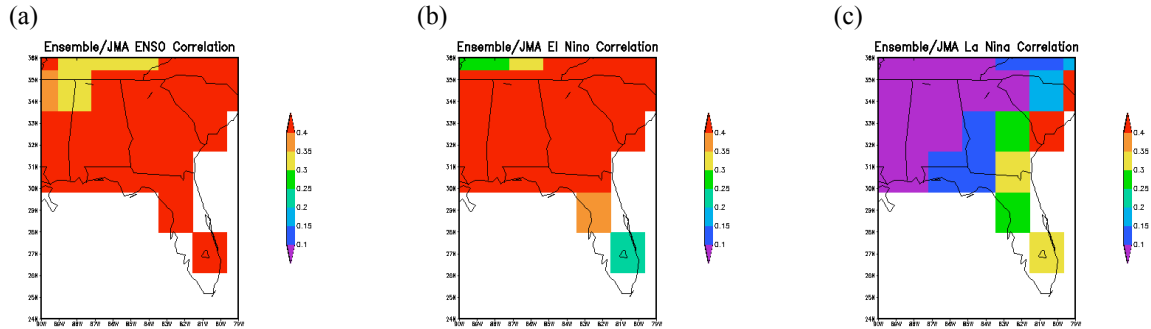


Figure 2: Temporal correlations of JMA box-averaged SSTs and observed precipitation for a) the overall ENSO signal, b) El Niño, and c) La Niña.

the ensemble ENSO signal correlations can be mostly attributed to El Niño. These correlations, particularly the ENSO signal and El Niño, show that the models are capable of recreating the spatial patterns of precipitation over the Southeast.

The Southeast is connected to the tropical Pacific through the upper level jet stream. The position of the jet stream over the Southeast changes with each ENSO phase. During El Niño, the jet stream shifts south over the warm waters of the tropical eastern Pacific and moves over the Gulf of Mexico. This allows for the moisture over the tropical eastern Pacific to reach the Southeast. During La Niña, the jet stream is more amplified over the western U.S. due to the shift in the warm pool westward over the tropical Pacific and thus takes a more northern track over the Southeast, shifting the maximum precipitation northward. Figure 2 shows the connection of the tropical Pacific SSTs to Southeast precipitation in the model ensemble for the overall ENSO signal, El Niño, and La Niña. As in Figure 1, El Niño appears to have a much stronger signal than La Niña in the models and thus influences the overall ENSO signal more. The problems with La Niña appear to lie in the model's ability to skillfully predict the SSTs over the tropical Pacific and therefore the jet stream.

4. Summary and Conclusions

Efforts to use models to predict Southeast precipitation patterns have emerged due to the connection of these patterns to ENSO. Using the FSUGSM, precipitation patterns are compared to observations to assess the skill of the model in predicting ENSO-related atmospheric phenomena. The model ensemble shows correlation values greater than 0.4 for the overall ENSO signal in coastal areas in the comparison to the observations and tropical Pacific SSTs. The model appears to have more skill in forecasting El Niño than La Niña, since both sets of correlations show lower values for La Niña than El Niño. This could be due to the model having problems with the position of the jet stream, particularly in La Niña. Future work consists of using a statistical test to verify the significance of the correlations.

Acknowledgements. We would like to thank D. W. Shin for the use of some of his data sorting codes and computer programming assistance. We would also like to thank Melissa Griffin for her assistance in the ongoing statistical test programming. This research is supported by the NOAA Office of Global Programs as an Applied Research Center to Dr. James J. O'Brien.

REFERENCES

- Cocke, S., and T. E. LaRow, 2000: Seasonal Predictions Using a Regional Spectral Model Embedded within a Coupled Ocean-Atmosphere Model. *Mon. Wea. Rev.* **128**, 689-708.
- Japan Meteorological Agency (JMA), Marine Department, 1991: Climate Charts of Sea Surface Temperatures of the Western North Pacific and the Global Ocean. 51 pp.
- Reynolds, R. W., and T. M. Smith, 1995: A High-Resolution Global Sea Surface Temperature Climatology. *J. Climate*, **8**, 1571-1583.
- Ropelewski, C. F., and M. S. Halpert, 1986: North American Precipitation and Temperature Patterns Associated with the El Niño/Southern Oscillation (ENSO). *Mon. Wea. Rev.*, **114**, 2352-2362.
- Willmott, C. J., and K. Matsuura, cited 2005: Terrestrial Air Temperature and Precipitation. [Available online at <http://climate.geog.udel.edu/~climate/>]

Quasioperational tests of the SL-AV model

Mikhail Tolstykh
Russian Hydrometeorological Research Centre,
and Institute of Numerical Mathematics Russian Academy of Sciences
Moscow Russia
Email: tolstykh@inm.ras.ru

The global finite-difference semi-Lagrangian model of Russian Hydrometeorological Research Centre (SL-AV) developed jointly with the Institute of Numerical Mathematics, Russian Academy of Sciences was described in [1, 2]. Its specific features include:

- semi-Lagrangian advection with SETTLS scheme, semi-implicit scheme with direct FFT solver;
- vorticity-divergence formulation on the unstaggered grid;
- fourth-order compact finite-difference schemes for horizontal derivatives, including semi-implicit scheme and U-V reconstruction.

The model resolution is 0.9x0.72 degrees (lon x lat), 28 sigma-levels. The SL-AV model uses parameterizations from Meteo-France ARPEGE/IFS model with minor modifications [3]. The model starts from the analyses produced by OI-based data assimilation system which uses the same model [4]. Among satellite data, only SATOB and some SATEM data are used.

Some results from quasioperational tests of the model during December 2004-August 2005 are presented in Fig. 1. For comparison, the results for Russian operational spectral Eulerian T85L31 model are also presented as well as the difference between two results. The scores for other regions demonstrate similar behavior, though the difference between two models is smaller; however, the scores for H500 at Northern extratropics at the range of 24 hours are better for spectral model.

It is necessary to keep in mind that somewhat different set of observations is used in OI analyses for both models. The analysis of the spectral model indirectly uses all satellite observations carried out 12 hours backwards. At the same time, SL-AV forecast starts 50 min later and at that time there are on average 5% more TEMP data and 10 % more AIREP data, the amount of SYNOP and SATOB data being the same.

Overall, the SL-AV model demonstrated advantage over Eulerian spectral model. However, the spurious orographic resonance occurred in some areas during test period, despite Eulerian treatment of orography and temporal uncentering. This resonance was eliminated by careful unification of fourth-order finite-differences and interpolation operators used throughout the model and also by changing the orography.

Based on these results, the constant resolution version of the SL-AV model was recommended for operational implementation.

This work was supported with Russian RFBR grant 04-05-64638.

REFERENCES

1. M.A. Tolstykh, Semi-Lagrangian high resolution model of the atmosphere for numerical weather prediction, Russian Meteorology and Hydrology, N4, 1-9 (2001).
2. M. Tolstykh, Vorticity-divergence semi-Lagrangian shallow-water model on the sphere based on compact finite differences, J. Comput. Phys. **179**, 180-200 (2002).

3. J.-F. Geleyn, E. Bazile, P. Bougeault et al, Atmospheric parameterization schemes in Meteo-France's ARPEGE N.W.P. model. In Parameterization of subgrid-scale physical processes, ECMWF Seminar proceedings (1994), 385-402.
4. M.D. Tsyroulnikov, M.A. Tolstykh, A.N. Bagrov, R.B. Zaripov, Development of a global data assimilation system with variable resolution, Russian Meteorology and Hydrology, N4, 5-24 (2003).

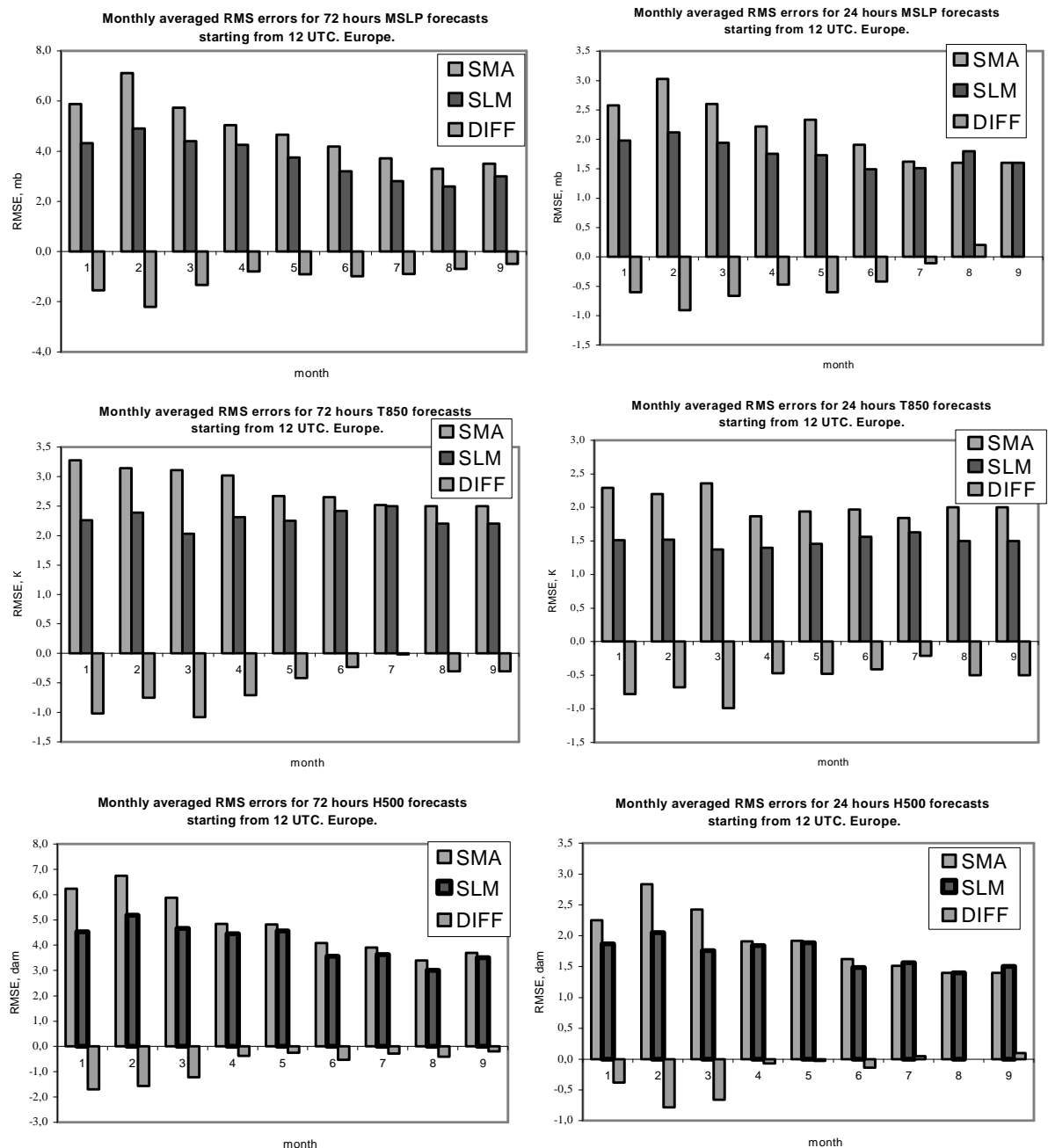


Fig.1 RMS scores for different variables and ranges of 72 hours (left) and 24 hours (right) over Europe for months between December 2004 (1) and August 2005 (9). SMA –RHMC Eulerian spectral model T85L31, SLM – SL-AV model, DIFF – difference between these models.